JGR Oceans

RESEARCH ARTICLE
10.1029/2024JC021113

Contribution of Anthropogenic and Lithogenic Aerosol Fe in the East China Sea

Chih-Chiang Hsieh[1,2] **and Tung-Yuan Ho**[1,2]

[1]Research Center for Environmental Changes, Academia Sinica, Taipei, Taiwan, [2]Institute of Oceanography, National Taiwan University, Taipei, Taiwan

Key Points:

- Anthropogenic aerosol Fe collected in the East China Sea mainly originates from high-temperature coal combustion of East Asia
- Cd to Ti ratio is a reliable proxy to quantify the contribution of total anthropogenic Fe in the coarse aerosols
- Lithogenic aerosol Fe is still the dominant source of aerosol dissolved Fe in the surface water of the East China Sea

Supporting Information:

Supporting Information may be found in the online version of this article.

Correspondence to:

T.-Y. Ho,
tyho@gate.sinica.edu.tw

Citation:

Hsieh, C.-C., & Ho, T.-Y. (2024). Contribution of anthropogenic and lithogenic aerosol Fe in the East China Sea. *Journal of Geophysical Research: Oceans*, *129*, e2024JC021113. https://doi.org/10.1029/2024JC021113

Received 14 MAR 2024
Accepted 18 NOV 2024

Author Contributions:

Conceptualization: Chih-Chiang Hsieh, Tung-Yuan Ho
Formal analysis: Chih-Chiang Hsieh, Tung-Yuan Ho
Funding acquisition: Tung-Yuan Ho
Investigation: Chih-Chiang Hsieh, Tung-Yuan Ho
Methodology: Chih-Chiang Hsieh, Tung-Yuan Ho
Project administration: Tung-Yuan Ho
Resources: Tung-Yuan Ho
Supervision: Tung-Yuan Ho
Validation: Chih-Chiang Hsieh, Tung-Yuan Ho
Writing – original draft: Chih-Chiang Hsieh, Tung-Yuan Ho
Writing – review & editing: Chih-Chiang Hsieh, Tung-Yuan Ho

Abstract Aerosol deposition is one of the major processes providing bioavailable Fe to the surface ocean. However, the quantification of aerosol Fe flux in the surface ocean is highly challenging operationally. In this study, we measured both Fe isotopic composition and specific elemental ratios in 5 size-fraction aerosols collected over the East China Sea (ECS) to quantify the relative contribution of lithogenic and anthropogenic aerosol Fe. Both the isotopic and elemental ratios indicate that anthropogenic aerosol Fe mainly originates from high-temperature combustion activities with the end member of the δ^{56}Fe to be −4.5‰. We found that the Cd/Ti ratio is a much more reliable proxy to quantify the contribution of anthropogenic aerosol Fe in coarse aerosols than δ^{56}Fe in the ECS. Attributed to extremely high deposition velocities and high total Fe concentrations for large size aerosols, lithogenic aerosols are still the dominant dissolved aerosol Fe source in the ECS.

Plain Language Summary The supply of iron to the surface oceans is a crucial factor deciding primary production and carbon cycling in the ocean. Traditionally, it was thought that natural dust was the primary contributor of both total and soluble aerosol iron to the surface oceans. However, some studies suggest that human-made aerosols could also play a significant role in supplying soluble Fe to surface waters. Yet, accurately estimating the flux of either natural or human-made aerosol Fe to the ocean surface is complex and challenging. During the winter and spring monsoon seasons, the East China Sea (ECS) receives substantial amounts of both natural and human-made aerosols from East Asia and serves as an ideal location to study the fluxes of natural and anthropogenic aerosol Fe. In this study, we used Fe isotopic analysis and elemental ratios of some specific elements in the ECS aerosols to estimate the relative contributions of anthropogenic and natural aerosol Fe. We found that in spite of the high anthropogenic aerosol input, natural dust remains the predominant supplier of soluble Fe to the surface waters in the ECS.

1. Introduction

The supply of dissolved Fe is a major factor influencing primary production and carbon cycling in the ocean (Martin, 1990; Tagliabue et al., 2017). Aeolian transport is one of the major Fe sources in the surface oceans in addition to other sources, such as continental shelves and hydrothermal vents (Lam & Bishop, 2008; Nishioka et al., 2007; Resing et al., 2015). Lithogenic aerosols have long been considered to be the major total and dissolved iron (Fe) source in the euphotic zone of the ocean (Jickells et al., 2016). However, some studies reported that anthropogenic aerosols, featured with extremely high Fe solubility, may play a significant role as dissolved Fe sources in the surface water (Conway et al., 2019; Luo et al., 2008; Mead et al., 2013; Sedwick et al., 2007). Using Fe isotopic composition to estimate the dissolved anthropogenic aerosol Fe (AN-Fe) fluxes, studies reported that the AN-Fe fluxes ranged from 20%–60% to 21%–59% of the dissolved Fe fluxes for the northwestern and subarctic Pacific regions, respectively (Kurisu et al., 2021; Pinedo-Gonzalez et al., 2020). However, it should be noted that the estimate of either lithogenic or anthropogenic aerosol Fe fluxes to the surface ocean is highly challenging and highly uncertain (Meskhidze et al., 2019; Myriokefalitakis et al., 2018). The uncertainties at least include the biases from the quantification of solubility, the evaluation of deposition velocities, the identification of aerosol Fe sources, the sampling procedures of size-fractionated aerosols, and the pre-and post-deposition transport processes of aerosols (Baker & Jickells, 2006; Hsieh et al., 2022; Perron et al., 2020; Wang & Ho, 2020).

In this study, we have applied both elemental and Fe isotopic composition to five size fractions of aerosol samples collected over the ECS to identify and quantify the sources of total and dissolved aerosol Fe. The ratios of certain specific metals to Ti are useful indicators of specific anthropogenic aerosol sources. For example, nickel (Ni) or vanadium (V) in aerosols are known to be associated with oil combustion (Nriagu & Pacyna, 1988; Sholkovitz

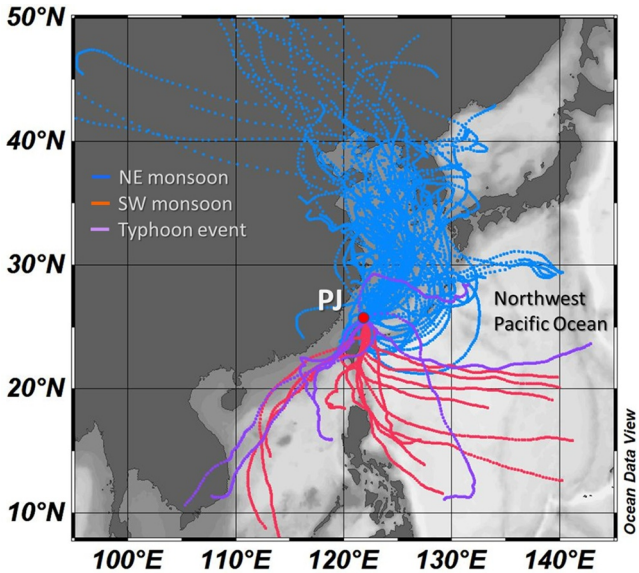

Figure 1. The location of the sampling station, Penjia islet (PJ), and 7-day air mass backward trajectory. The red, blue, and purple lines stand for southwestern monsoon, northeastern monsoon, and typhoon events, respectively.

et al., 2009). Potassium (K) in fine aerosols is known to be an indicator for biomass, wildfire, and fossil fuel burning (Andreae, 1983; Perron et al., 2022). Aerosol sulfur (S) mainly originates from coal combustion in East Asia (Lin et al., 2015, 2022). The elements cadmium (Cd), zinc (Zn), and lead (Pb) are also enriched in fossil fuel combustion processes (Nriagu & Pacyna, 1988). However, the EF of size-fractionated aerosol Fe does not exhibit significantly different ratios (Buck et al., 2019; Hsieh et al., 2023). For example, although the EF_{Cd} ranged over 3 orders of magnitude from 3.1 to 2,873, the EF_{Fe} only ranged from 1.2 to 3.4 in the 5 size fraction aerosols collected in the ECS (Hsieh et al., 2023). Fe isotopic composition in different size aerosols may provide independent evidence to trace the sources of aerosol Fe and estimate their contribution. The δ^{56}Fe value of lithogenic dust and loess, which have been thoroughly studied typically with values around +0.10 ± 0.10‰ (Beard et al., 2003; Fitzsimmons & Conway, 2023; Waeles et al., 2007). The δ^{56}Fe values in lithogenic aerosols do not significantly change during atmospheric transport processes (Conway et al., 2019; Gong et al., 2016). In terms of AN-Fe isotopic features, it has been reported that fossil fuel with high-temperature combustion can cause significant Fe isotope fractionation during evaporation and yield much lower δ^{56}Fe, as low as −3.2‰ for total fine aerosols (Kurisu, Sakata, et al., 2016). Similarly, the temperature level in smelting activities is also extremely high, generally ranging from 1,000 to 2,000°C, and the δ^{56}Fe value in the emitted aerosols is relatively light down to −3.5‰ and −3.9‰ for toal and ultrapure water leaching fine aerosols (<0.7 μm) (Kurisu et al., 2019). The δ^{56}Fe value of high temperature combustion Fe is suggested to range from −3.9 to −4.7‰ (Kurisu, Takahashi, et al., 2016; Kurisu et al., 2019). Kurisu and Takahashi (2019) observed insignificant Fe fractionation in aerosols collected from biomass burning and proposed that it may be attributed to relatively low combustion temperature or the suspension of soil particles. Overall, the isotopic composition and fractionation of Fe in fly ashes originated from biomass burning still remain unclear. Without significant isotopic fractionation among different anthropogenic aerosol Fe sources, δ^{56}Fe alone may not be useful to distinguish and quantify the sources. The coupling information of δ^{56}Fe and some specific elemental ratios shall be beneficial to distinguish the sources (Conway et al., 2019).

The East China Sea (ECS), receiving large amounts of both anthropogenic and lithogenic aerosols from East Asia during the northeastern monsoon seasons, provides an excellent location to investigate the relative contribution of different sources of aerosol Fe (Figure 1). We determined both δ^{56}Fe and various elemental ratios of proxy elements to estimate the contribution of different aerosol sources for total and dissolved aerosol Fe for both masses and fluxes from 5 size-fraction aerosols collected in the ECS. The aerosol leaching Fe include ultrapure water and buffer leached Fe using the procedures proposed (Perron et al., 2020). The findings of this study shall shed insights on the relative contribution of lithogenic and anthropogenic aerosols Fe in oceanic surface water regionally and globally.

2. Method

2.1. Sampling Site and Procedures

The aerosol samples were collected in a small islet in the ECS, Pengjia islet (PJ, 1.1 km^2, 25.63°N, 122.08°E), which is located at 66 km north of the northernmost point of Taiwan (Figure 1). There are only about 30 governmental staff stayed on the volcanic islet for meteorological observation and coastal guarding. Based on aerosol optical depth data, PJ receives aerosols from the north during the northeast monsoon season and from the south during the southwest monsoon season (Figure 1). This makes it an ideal time series sampling site to investigate the impact of East Asian aerosols on the surface water of the northwestern Pacific Ocean (NWPO). Size-fractionated aerosol samples were collected by polytetrafluorethylene filters (TE-230-PTFE, Tisch Environmental Inc., US) installed on the high volume aerosol sampler (TISCH Environmental Inc., US, MODEL-TE-5170) and coupled with a cascade impactor (TISCH Environmental Inc., US, Series 235). The cascade impactor separated aerosols into five size fractions, including stage 1 (>7.3 μm), stage 2 (3.1–7.3 μm), stage 3 (1.6–3.1 μm), stage 4 (1.0–1.6 μm), and stage 5 (0.57–1.0 μm). The stage 5 and stage 1–4 aerosols are referred to as fine

and coarse aerosols in this study, respectively. The collection time for one single filter generally lasted for 7–8 days each month from September 2019 to August 2020 to ensure sufficient mass for isotopic composition analysis in different treatments. Detailed sampling information, including sampling dates and volumes, is shown in Table S1 of Supporting Information S1. The filters with aerosol samples were freeze-dried and weighed after collection. The aerosol samples were then stored at −20°C freezer prior to further chemical processing.

2.2. Quantification of Dissolved and Total Concentrations and Isotopic Composition

All sample pretreated procedures were carried out in an ISO Class 4 positive pressure cleanroom by operators wearing powder-free polyvinyl chloride (PVC) gloves. We followed the suggested protocols of GEOTRACES Cookbook to clean sample vials (Cutter et al., 2017). Regarding the dissolved fraction, we conducted two different leaching protocols, including instantaneous ultrapure water leached (ultrapure water) and acetate buffer leached (buffer) treatments. The ultrapure water Fe was obtained by passing ultrapure water through 0.2 μm filters instantaneously (Buck et al., 2006; Morton et al., 2013). For buffer leached Fe (buffer Fe), an ammonia acetate buffer solution at pH 4.7 was used to mimic aerosol metals dissolution processes by rainwater (Baker & Jickells, 2006; Sarthou et al., 2003) or short period complexation processes by seawater ligands (Perron et al., 2020). For total digestion (referred as "total" hereafter), samples were heated for 4 hr at 120°C (heater temperature) in 2 ml of a freshly prepared mixed solution containing 4M HF, 4M HCl, and 4M HNO_3 (Eggimann & Betzer, 1976). Solubilities were calculated by dividing the concentrations of elements leached with either Milli-Q water or buffer by their total concentrations. Filter blanks for each treatment were obtained by subjecting new filters to the same leaching procedures as the samples. In over 90% of the cases, the sample concentrations were at least two orders of magnitude higher than the concentrations of the blanks, and in all cases, the samples were at least one order of magnitude higher than the blank value. The detailed information about the pretreatment procedures, analytical method, blank test, and the validation of precision and accuracy were described in our previous studies (Hsieh et al., 2022, 2023).

Iron isotopic compositions were determined by using multi-collector inductively coupled plasma mass spectrometer (MC-ICP-MS, Neptune Plus, Thermo Fisher Scientific) equipped with a sample inlet system APEX-IR (no gas added), normal Ni sampler cone, and X-type skimmer cone from elemental scientific. Samples were measured in high-resolution mode with ^{54}Cr correction on ^{54}Fe and ^{58}Ni correction on ^{58}Fe. The $\delta^{56}Fe$ measurements were conducted using the double-spike technique, involving the addition of mixed spike (^{57}Fe and ^{58}Fe) with a sample-to-spike ratio of 1:2, as described by Dauphas et al. (2017). The $\delta^{56}Fe$ data ($^{56}Fe/^{54}Fe$) ratios are reported in per mil notation (‰) relative to the IRMM-014 Fe isotope reference material (Institute for Reference Materials and Measurements) and described below:

$$\delta^{56}\mathrm{Fe}\,(‰) = \left(\frac{\left(^{56}\mathrm{Fe}/^{54}\mathrm{Fe}\right)_{\mathrm{sample}}}{\left(^{56}\mathrm{Fe}/^{54}\mathrm{Fe}\right)_{\mathrm{IRMM-014}}} - 1\right) \times 1000$$

To minimize the Cr and Ni interferences, we purified all samples using an anion exchange resin (AG1-X8, Bio-Rad, 100–200 mesh). The samples were loaded in 1.4 mL 7 N HCl solution onto perfluoroalkoxy alkanes (PFA, Savillex) microcolumns filled with the resin. We then applied ultrapure 0.4 ml 7N HCl thrice to remove Ni and Cr. The Fe was retained on the resin and later eluted out with 0.7 N HCl (Figure S1 in Supporting Information S1). The eluted off purified Fe samples were dried in open cap vials then redissolved subsequently in 1 ml of 0.5 M HNO_3 at 120°C for 2 hr with closed caps and then were ready for isotopic analysis. We measured IRMM-014 every 4 sample analyses and measured NIST-3126a every 8 sample analyses to validate analytical accuracy. Our long-term $\delta^{56}Fe$ value of NIST-3126a is 0.36 ± 0.03‰ ($n = 25$), averaged from 5 different analytical periods spanning for half year. This value is comparable to the value reported in previous studies 0.36 ± 0.04‰ by Sieber et al. (2021), 0.35 ± 0.06‰ by Stevenson et al. (2017), and 0.39 ± 0.13‰ reported by Rouxel and Auro (2010). The precision and accuracy of $\delta^{56}Fe$ data in this study were validated using reference materials BCR2 and BHVO2 (Table 1 (Craddock & Dauphas, 2010)).

Table 1
Precision and Accuracy Validation of δ^{56}Fe Using Reference Material BCR2 and BHVO2

Reference material	Purification blank[a] (ng) (n = 5)	Digestion concentration recovery (%) (n = 5)	Purification recovery (%) (n = 5)	δ^{56}Fe (‰) This study[a] (n = 5)	δ^{56}Fe (‰) Craddock, Dauphas, 2010
BCR2	0.22 ± 0.05	99 ± 1	94 ± 3	0.11 ± 0.02	0.13 ± 0.03
BHVO2	0.22 ± 0.05	98 ± 1	99 ± 5	0.09 ± 0.02	0.11 ± 0.02

[a]All of the samples were processed by the elution procedures twice (Figure S1 in Supporting Information S1) to purify Fe. The values of the errors represent one standard deviation of 5 replicate CRM samples through pretreatment and analysis.

3. Result

3.1. Size and Seasonal Variations of δ^{56}Fe

The 7-day air mass backward trajectory analysis showed that the air mass transport pathways were generally opposite between the northeastern monsoon (NE) season and the southwestern monsoon (SW) season (Figure 1). Aerosols generally originated from East Asia during the NE monsoon seasons from September 2019 to May 2020; aerosols mainly came from the oceanic region in the south during the SW monsoon seasons from June 2020 to July 2020 (Figure 1). We did not include the August sample into the SW season since category 4 typhoon Maysak passed through the ECS in August 2020. Our previous studies found that the concentrations of total Fe increased with increasing particle sizes and the concentrations of ultrapure water leached Fe exhibited opposite patterns with aerosol sizes (Hsieh et al., 2022, 2023). The differences between total Fe and ultrapure water leached Fe increased with increasing particle sizes and were up to three orders of magnitude for size 7.3 μm. The solubilities of ultrapure water leached Fe varied up to four orders of magnitude with the size spectrum and exhibited a highly linear correlation with non-sea-salt sulfur. In terms of the seasonality, we did not observe significant differences in concentration or Fe solubility. The seasonal variations of total, ultrapure, and buffer δ^{56}Fe in the size-fractionated aerosol samples are also shown in Figure 2. The total Fe isotope composition remained relatively consistent for the three larger aerosols with values ranging from +0.10 to −0.08‰, +0.16 to +0.00‰, and +0.14 to −0.06‰ for size cut-offs 1.6, 3.1, and 7.3 μm, respectively (Figure 2). However, for the two smallest size aerosols, δ^{56}Fe sharply decreased with decreasing sizes with value ranging from −0.45 to −3.35 to −0.06 to −1.16‰ for size cut-offs 0.57 and 1.0 μm, respectively (Figure 2, Table 2). For the seasonality in total δ^{56}Fe composition, the averaged values of the 2 smallest size aerosols collected during NE seasons were −2.19 ± 0.91‰ and −0.54 ± 0.41‰ for size cut-offs 0.57 and 1.0 μm, respectively, which were significantly lower than the value obtained in SW seasons, −0.66 ± 0.29‰ and −0.15 ± 0.04‰ (Table 2). The August δ^{56}Fe

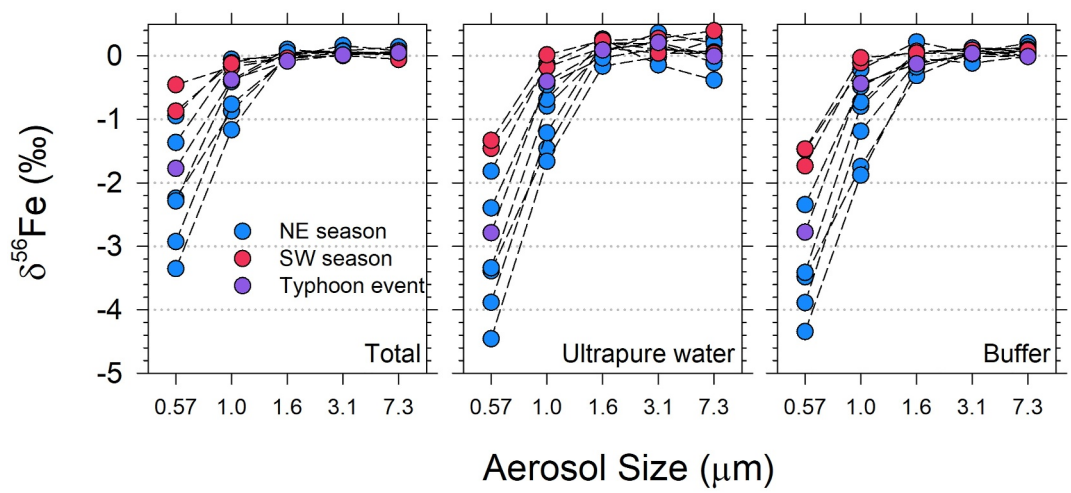

Figure 2. The seasonal total ultrapure water leached and buffer leached δ^{56}Fe compositions of the size-fractionated aerosols collected in the ECS. As the analytical error was relatively small (0.04 ± 0.01‰) compared to the differences between the samples, the error bars were not shown in the figure.

Table 2
The δ^{56}Fe Compositions of Total, Ultrapure Water Leached, and Buffer Leached of the Size-Fractionated Monthly Aerosol Samples Collected in the ECS

Size cut-offs (μm)	Leaching fraction	δ^{56}Fe (‰)									
		September	December	January	February	March	April	May	June	July	August
0.57	Ultrapure	−3.39 (0.06)[a]	−4.46 (0.05)	*−3.88*[b] *(0.07)*	*−1.82 (0.08)*	−3.34 (0.04)	n.a.[c]	*−2.40 (0.08)*	*−1.46 (0.09)*	−1.33 (0.05)	−2.79 (0.05)
	Buffer	−3.48 (0.04)	−4.34 (0.05)	−3.89 (0.04)	−1.48 (0.05)	*−3.41 (0.08)*	n.a.	−2.34 (0.03)	−1.73 (0.05)	−1.47 (0.04)	−2.78 (0.04)
	Total	−2.24 (0.04)	−3.35 (0.03)	−2.93 (0.04)	−0.94 (0.04)	−2.29 (0.05)	n.a.	−1.36 (0.04)	−0.45 (0.04)	−0.87 (0.05)	−1.77 (0.03)
1.0	Ultrapure	−1.46 (0.04)	−1.66 (0.04)	*−1.21 (0.08)*	*−0.13 (0.09)*	−0.79 (0.03)	*−0.68 (0.07)*	*−0.46 (0.08)*	*−0.18 (0.08)*	0.01 (0.05)	−0.40 (0.04)
	Buffer	−1.74 (0.06)	−1.88 (0.04)	−1.19 (0.04)	−0.22 (0.05)	*−0.79 (0.06)*	*−0.73 (0.07)*	−0.48 (0.05)	−0.11 (0.05)	−0.03 (0.05)	−0.44 (0.05)
	Total	−0.87 (0.05)	−1.16 (0.04)	−0.76 (0.05)	−0.06 (0.04)	−0.41 (0.04)	−0.38 (0.04)	−0.11 (0.03)	−0.18 (0..04)	−0.12 (0.04)	−0.38 (0.04)
1.6	Ultrapure	0.08 (0.06)	−0.16 (0.03)	*0.20 (0.09)*	*0.26 (0.09)*	0.06 (0.04)	*0.22 (0.09)*	*−0.03 (0.11)*	*0.13 (0.08)*	0.24 (0.06)	0.09 (0.04)
	Buffer	−0.31 (0.09)	−0.18 (0.04)	−0.09 (0.04)	0.22 (0.04)	*0.03 (0.06)*	*0.05 (0.07)*	−0.04 (0.04)	0.07 (0.05)	0.04 (0.03)	−0.13 (0.05)
	Total	−0.02 (0.03)	0.03 (0.04)	−0.04 (0.04)	−0.02 (0.03)	0.05 (0.04)	0.10 (0.05)	0.05 (0.06)	−0.04 (0.07)	−0.04 (0.06)	−0.08 (0.04)
3.1	Ultrapure	0.23 (0.03)	−0.02 (0.06)	*0.19 (0.07)*	*0.14 (0.08)*	0.36 (0.05)	*0.10 (0.09)*	*−0.11 (0.10)*	*0.04 (0.09)*	0.27 (0.05)	0.21 (0.04)
	Buffer	0.05 (0.05)	0.05 (0.04)	−0.01 (0.04)	0.04 (0.03)	*0.12 (0.07)*	*0.12 (0.07)*	−0.12 (0.04)	0.09 (0.04)	0.03 (0.05)	0.04 (0.04)
	Total	0.04 (0.05)	0.06 (0.04)	0.05 (0.05)	0.16 (0.04)	0.08 (0.05)	0.03 (0.04)	0.07 (0.04)	0.00 (0.05)	0.01 (0.05)	0.01 (0.04)
7.3	Ultrapure	0.28 (0.08)	0.25 (0.07)	*−0.11 (0.10)*	*0.38 (0.09)*	0.20 (0.04)	*0.06 (0.10)*	*0.03 (0.13)*	*0.04 (0.09)*	0.40 (0.06)	0.00 (0.04)
	Buffer	0.20 (0.05)	0.14 (0.05)	0.00 (0.04)	0.05 (0.06)	*0.06 (0.06)*	*0.10 (0.07)*	−0.01 (0.05)	0.00 (0.03)	0.08 (0.04)	−0.01 (0.04)
	Total	0.01 (0.05)	0.06 (0.04)	0.04 (0.02)	0.08 (0.04)	0.14 (0.03)	0.03 (0.05)	0.03 (0.04)	0.08 (0.05)	−0.06 (0.05)	0.05 (0.03)

[a]The values in parentheses represent the analytical error (2 standard deviations). [b]We observed abnormal MC-ICPMS isotopic signals for certain samples analyzed, which are highlighted in italics. To address this, we redigested the purified samples overnight (approximately 12 hr) and subsequently obtained stable and consistent isotopic signals. [c]n.a: Samples are not available.

value for 0.57 μm fraction was relatively low, −1.8‰, which was supposedly attributed to elevated anthropogenic aerosol input brought to the PJ by Maysak typhoon with radius up to 100 km.

In terms of ultrapure water and buffer leached samples, the deviation pattern among different size aerosols is similar to total samples with consistent values for the three large sizes and significantly lower values for the two small size aerosols. However, compared to total digestion samples, we found that the value observed in ultrapure water and buffer fractions were significantly lower than the value of total digestion for size cut-offs 0.57 and 1.0 μm. The deviations for ultrapure water and buffer leached samples from the total samples were 0.96 to 0.97‰ for size cut-offs of 0.57 μm and were 0.25 and 0.32‰ for size cut-offs of 1.0 μm, respectively (Figure 2, Table 2).

4. Discussion

4.1. Two End Member Mixing: Evidence From Elemental Ratios and δ^{56}Fe

Regarding elemental ratios, titanium (Ti) has proven to be a more reliable tracer of lithogenic material in aerosols than aluminum (Al). For example, in high lithogenic aerosol loading samples collected over the Pacific Ocean (GEOTRACES GP-15 cruise), Fe/Al ratios were significantly deviated from mean upper continental crust values than Fe/Ti ratios (Marsay et al., 2022). Figure 3 shows the correlations between the Ti-normalized ratios of the five elements and Fe and δ^{56}Fe in total aerosols. All of the ratios exhibit a negative linear correlation with δ^{56}Fe in the two finer size aerosol fractions. Although we did observe high non-sea-salt (nss-) K to Ti ratios, it is unclear whether the extremely low δ^{56}Fe originate from low temperature biomass burning aerosols or not. Similarly, as V/Ti ratios in heavy fuel oil aerosol emissions ranging from 120 to 1,000 mol mol^{-1} (Basha et al., 2020; Streibel et al., 2017), the relatively low V/Ti ratios observed indicate that heavy oil burning is unlikely to be the major source of fine aerosol Fe.

The ratios of Cd and Pb exhibited relatively high linear correlation with δ^{56}Fe among the six elements with correlation coefficients of 0.94 and 0.84, respectively. Although both Cd and Pb have low melting/boiling temperatures, 321/767 and 327/1,749°C, respectively, these two metals in fly ash mainly originate from high-

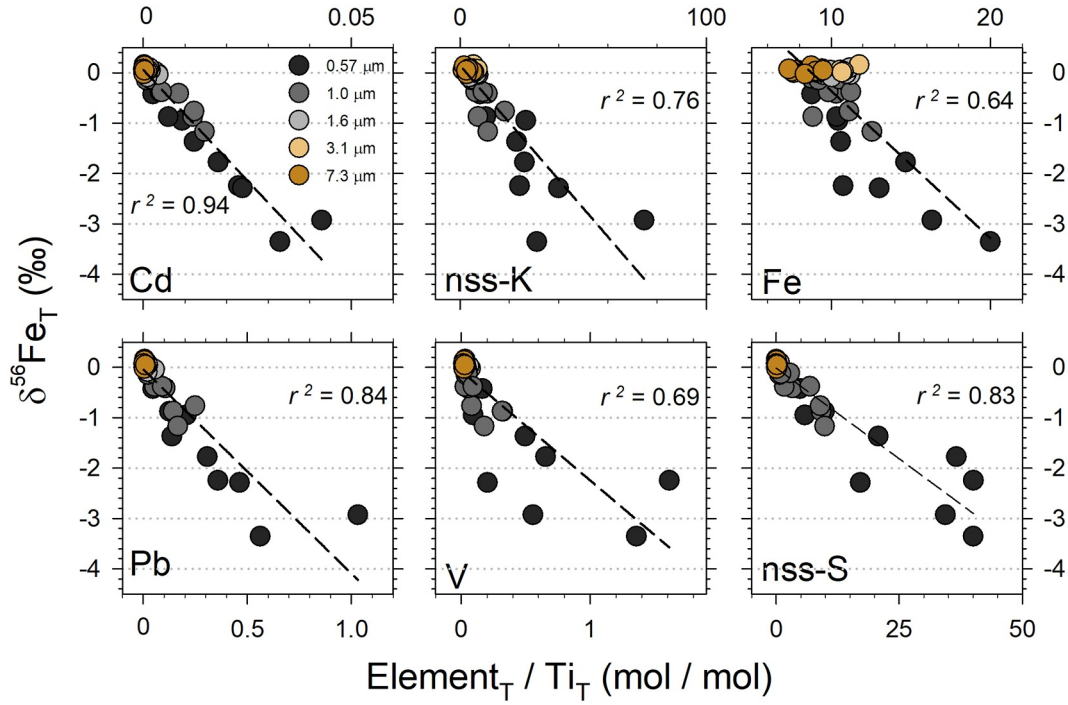

Figure 3. The correlation between elemental ratios (to Ti) and δ^{56}Fe for total treatment in the size-fractionated samples.

temperature combustion anthropogenic activities, including coal and oil burning, metal smelting and refining, and waste incineration. The two metals would thus be evaporated, condensed, aggregated, and adsorbed on flying ashes so that they are highly enriched in fine anthropogenic aerosols. Based on the strong correlation between Cd/Ti (and Pb/Ti) and δ^{56}Fe (Figure 3), Cd/Ti and Pb/Ti ratios may be useful to quantify the contribution of AN-Fe in the studied region. Our two-end members mixing assumption for aerosol Fe (anthropogenic and lithogenic aerosol Fe) is also strongly supported by the high correlation observed between decreasing δ^{56}Fe and increasing Cd (and Pb) to Ti ratios. The lowest δ^{56}Fe value observed in the smallest size (0.57 μm) aerosol in this study was −3.35‰ comparable to the values reported in previous studies for aerosol samples collected in heavy traffic or near steel plants, −3.2‰ and −3.5‰, respectively (Kurisu, Sakata, et al., 2016; Kurisu et al., 2019). Our low δ^{56}Fe values in the fine aerosols are consistent with the high-temperature fossil fuel combustion. The strong correlation (r^2 = 0.83) between δ^{56}Fe and nss-S/Ti further supports that fly ash from coal burning is the major source of fine aerosol Fe (Figure 3).

Since dissolved Fe obtained from ultrapure water and buffer leached treatments in fine aerosol mainly originates from AN-Fe, the isotopic value of the dissolved Fe would thus be close to the end member of anthropogenic aerosol Fe. The lowest values measured in this study were −4.46 and −4.34‰ in the ultrapure water and buffer Fe fractions, respectively (Figure 3, Table 2). Derived from high-temperature combustion, Kurisu et al. (2019) suggest the isotopic composition of AN-Fe aerosols in East Asia shall fall between −3.9 and −4.7‰. Conway et al. (2019) proposed an isotopic range from −1.6 to −1.8‰ as the end member of AN-Fe in the North Atlantic Ocean. In this ECS study, we then used the lowest δ^{56}Fe value observed in our studied region as the end member of AN-Fe, which is −4.4‰. As the intercept of y axis for the δ^{56}Fe versus Cd/Ti plot is +0.06‰ (Figure 3) also comparable to the typical δ^{56}Fe range of lithogenic aerosols (+0.10 ± 0.10‰) (Beard et al., 2003; Conway et al., 2019; Mead et al., 2013; Waeles et al., 2007), we thus use +0.1‰ as the end member of lithogenic aerosols. Based on the correlation between δ^{56}Fe and Cd/Ti ratios, the estimated end members of Cd/Ti and Pb/Ti ratios in anthropogenic aerosols would be 50 and 1,030 mmol mol^{-1}, respectively (Figure 3).

4.2. δ^{56}Fe Versus Fe Solubility

We further compared δ^{56}Fe in total size fractionated aerosols with aerosol Fe solubilities obtained with ultrapure water and buffer leaching treatments (Figures 4a–4d). A significant linear correlation was observed between total

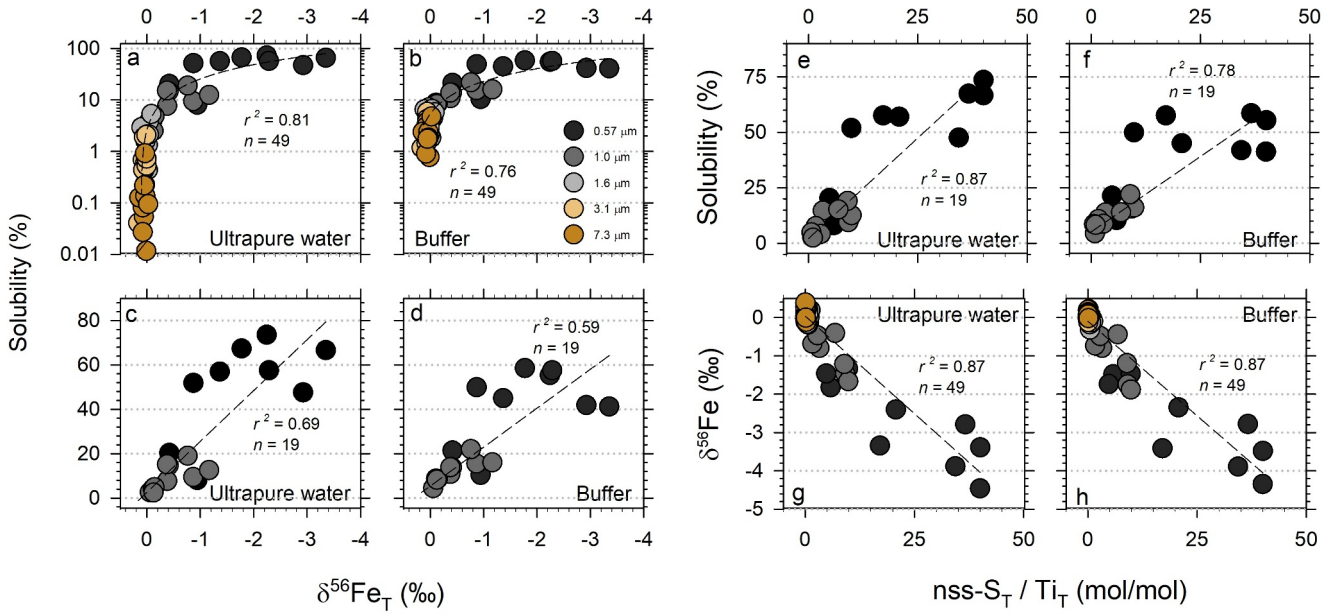

Figure 4. (left) The correlation of total aerosol δ^{56}Fe with Fe solubility in size-fractionated aerosols (right) The comparison between nss-S to Ti ratio with Fe solubility and δ^{56}Fe obtained by ultrapure water and buffer leached.

δ^{56}Fe and the solubilities of ultrapure water and buffer aerosol Fe with correlation coefficients (r^2) to be 0.81 and 0.76, respectively, demonstrating that dissolved Fe mainly originated from anthropogenic aerosols. The overall ultrapure water solubilities varied up to four orders of magnitude for all of the five size samples, and the isotopic values of total Fe varied by about 3.6‰, ranging from +0.16 to −3.4‰. However, the ultrapure water Fe solubilities for aerosol sizes from 1.6 to 7.3 μm varied up to two orders of magnitude (0.01%–5.4%) but δ^{56}Fe only ranged from +0.16 to −0.08‰ (Figure 4a). Due to the relatively large uncertainty for Fe isotopic analysis (0.04‰), the variability of δ^{56}Fe for larger fractions aerosols (7.3, 3.1, and 1.6 μm) was within or close to analytical uncertainty value and was too small to effectively quantify the contribution of anthropogenic aerosols. Instead, the Cd/Ti ratios for the three larger size aerosols also varied up to two orders of magnitude, 0.04–3.62 mmol mol^{-1} (Hsieh et al., 2023), and Cd/Ti and Pb/Ti also exhibited high correlation in three larger fractions (Figure 5d). Thus, Cd/Ti ratios are a much more sensitive and reliable parameter to represent the contribution of anthropogenic aerosol (Fe) than Fe isotopic ratio in this study.

Assuming two-end-member mixing and using the end member value of Cd/Ti ratios observed in anthropogenic aerosol (50 mmol mol^{-1}) (Figure 3) and in the lithogenic dust (0.012 mmol mol^{-1}) (Hu & Gao, 2008), we thus estimated δ^{56}Fe for the highest Cd/Ti value in the three coarser fractions. The estimated value is −0.14‰, which is quite close to the value measured (−0.08‰). Assuming the end member of Fe solubility to be 80% (Figure 4a), the predicted or estimated solubility for the sample (−0.08‰) is 5.4%, which is also relatively close to the value observed, 3.7%. Further studies are needed to validate the value of applying Cd/Ti ratios as a proxy to estimate the contribution of AN-Fe and Fe solubility.

The strong linear correlation between Cd/Ti ratios and low δ^{56}Fe for PM 1.0 strongly supports that the PM 1.0 was driven by lithogenic and anthropogenic aerosols two end members mixing (Figure 3). However, the correlation between solubility and δ^{56}Fe in the two finest fractions was relatively poor (Figures 4c and 4d) with solubilities varying from 2.5% to 74%, and δ^{56}Fe varying from −0.11 to −3.4‰. We argue that other physical and chemical conditions may be important in influencing the solubilities. For example, nss-S/Ti exhibits better correlations with the solubilities of ultrapure water and buffer leached Fe than δ^{56}Fe (Figures 4e and 4f), suggesting that inorganic acid concentrations in aerosol samples are a critical factor controlling Fe solubility. Other potential factors may include the availability of organic acids, inorganic, and organic ligands in different types or speciation of anthropogenic particles or the strength of solar radiation and in-cloud processes.

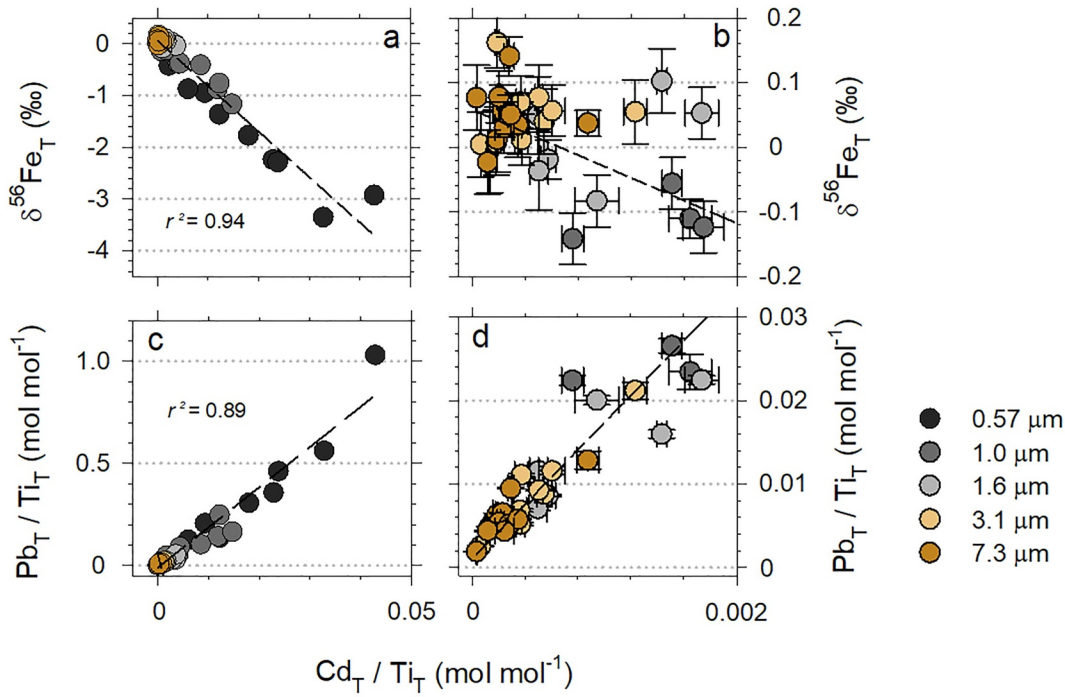

Figure 5. The correlation between δ^{56}Fe, Cd/Ti, and Pb/Ti ratios for total digestion samples. The correlation coefficients of plots b and d for the two coarse fractions are 0.0013 and 0.86, respectively.

4.3. Quantify AN-Fe by Using δ^{56}Fe and Cd/Ti Ratio

Using +0.10/−4.4‰ and 0.012/50 mmol mol^{-1} as the two end members of δ^{56}Fe and Cd/Ti ratios in lithogenic aerosol Fe and AN-Fe, respectively, we quantified the relative contribution of each end member by a two-component mixing model for each size fraction (Conway et al., 2019; Ho & Hsieh, 2024; Kurisu et al., 2021) (Table 3 and Tables S2 and S3 in Supporting Information S1):

$$Fe_{measured} = Fe_{dust} \times f_{dust} + Fe_{anthropogenic} \times f_{anthropogenic}$$

The terms of Fe_{dust} and $Fe_{anthropogenic}$ stand for end member values, either δ^{56}Fe or Cd/Ti ratios, for dust and fossil fuel high-temperature combustion aerosols. $Fe_{measured}$ stands for the δ^{56}Fe or Cd/Ti ratios measured in each size fraction. The terms, f_{dust} and $f_{anthropogenic}$, stand for the fractions of the aerosol sources in the total aerosol, with sum to be one or 100%. We then quantified the two fraction terms using either δ^{56}Fe or Cd/Ti ratios for each aerosol size of all of the samples measured. We found that the contribution estimated by Cd/Ti ratio for total AN-Fe is comparable to the value obtained by δ^{56}Fe among size cut-offs 0.57–1.0 µm (Ho & Hsieh, 2024) ($r^2 = 0.92$, Table 3, Table S3 in Supporting Information S1). The two comparable values, obtained by two independent

Table 3
The Estimated Contribution of Anthropogenic Aerosol Fe for Concentrations and Fluxes Using Two Independent Estimation Approaches (δ^{56}Fe vs. Cd/Ti) in the Two Representative Months of NE and SW Monsoon Seasons, Respectively

AN-Fe estimated approach		NE (December 2019)			SW (July 2020)		
		Ultrapure	Buffer	Total (%)	Ultrapure	Buffer	Total (%)
By δ^{56}Fe	Conc.	85%	40%	7.6	22%	10%	3.5
	Flux	32%	0.7%	1.1	0.1%	0.8%	3.1
By Cd/Ti	Conc.	n.a.	n.a.	7.3	n.a.	n.a.	0.9
	Flux	n.a.	n.a.	0.7	n.a.	n.a.	0.3

Note. *n.a: data are not available. The deposition velocities used in the flux calculation are based on Hsieh et al. (2022).

approaches, validate the two end member assumption and the accuracy of the estimates. In terms of the two coarse sizes, δ^{56}Fe shows poor correlation with Cd/Ti ratio ($r^2 = 0.0013$, Figure 5b). However, Cd/Ti ratios still maintain a strong linear correlation ($r^2 = 0.86$) with Pb/Ti in coarse aerosols with the same slope as fine aerosols (Figure 5d). Not only the elemental ratios varying up to a few orders of magnitude in the size-fractionated aerosols but their concentrations were relatively high and can be measured precisely, the elemental ratios thus were relatively reliable proxies to estimate the contribution of anthropogenic aerosols in comparison with δ^{56}Fe particularly for coarse sizes. In brief, δ^{56}Fe is not a reliable parameter to estimate the contribution of AN-Fe in coarse aerosols. The strong and same linear correlation between Cd/Ti and Pb/Ti in both fine and coarse aerosols indicates that both Cd and Pb in coarse aerosols still originated from anthropogenic aerosols (Figure 5). Although the δ^{56}Fe values in coarse aerosols were generally close to lithogenic aerosol Fe, the possible contribution of AN-Fe in the coarse fraction should not be fully excluded. The dissolved Fe in coarse fraction of lithogenic aerosols may also be impacted by the anthropogenic aerosols.

The average total mass contributions of AN-Fe for the two finest aerosols (0.57/1.0 μm) would be 51/14% and 17/5.6% for the NE and SW monsoon seasons, respectively (Table S2 in Supporting Information S1 (Ho & Hsieh, 2024)). However, the averaged AN-Fe mass only accounts for 5.2% and 2.7% of total aerosol mass during the NE and SW monsoon seasons, respectively. Using the December sample as an example, AN-Fe contributed 7.8%, 41%, and 87% of Fe for total, buffer, and ultrapure water masses, respectively (Table 3). In terms of flux estimates, we have calculated the deposition fluxes by multiplying size-fractionated aerosol Fe concentrations with size specific deposition velocities. Considering size and atmospheric condition specific deposition velocities (Hsieh et al., 2022), the AN-Fe flux contributions were only 1.1% and 1.4% for total and buffer treatments and 34% for ultrapure water leached treatment, respectively, in December (Table 3). Using the same two-end member approach by Cd/Ti ratios, the contribution of AN-Fe in total Fe was only 0.7%, which is similar to the value estimated by δ^{56}Fe approach (Table 3). These estimates are only for aerosol dry deposition. In terms of wet deposition, since the scavenging ratio of coarse aerosols are much higher than fine aerosols in wet deposition (Duce et al., 1991), coarse aerosols would also account for a higher contribution than fine aerosol for aerosol Fe wet deposition fluxes in our studied region. Supposedly, AN-Fe would still account for a minor contribution in wet deposition.

5. Conclusion

The lowest δ^{56}Fe values of total, buffer, and ultrapure water leaches were −3.35, −4.46, and −4.34‰, respectively, indicating that AN-Fe in the aerosols originated from high-temperature combustion. Using the elemental and isotopic end members, we have quantified the relative contribution of lithogenic and anthropogenic aerosol Fe. We also found that Cd/Ti ratio is a sensitive and reliable proxy to quantify the contribution of total AN-Fe in coarse aerosols collected in the ECS. Although anthropogenic aerosols are a major source of dissolved Fe concentrations in fine aerosols, lithogenic aerosols are still the dominant source of ultrapure water, buffer, and total Fe in the surface water of the ECS and its marginal seas.

Data Availability Statement

Monthly meteorological conditions during the sampling periods was obtained from the Weather Bureau of Taiwan at https://e-service.cwb.gov.tw/HistoryDataQuery/index.jsp. The iron isotope and elemental ratio data (Cd/Ti) used to estimate the contributions of anthropogenic and lithogenic aerosol Fe in this study has been published in the Dryad data repository (Ho & Hsieh, 2024). The data set is archived at Dryad, https://doi.org/10.5061/dryad.rv15dv4h3, and is also accessible in the Supplementary files.

Acknowledgments
We sincerely appreciate the invaluable comments provided by the two anonymous reviewers and the associate editor. We appreciate the technical support of H.-Y. Chen and K.-P. Chiang and the comments of S.-C. Pai, C.-F. You, Y.-T. Hsieh, Y.-C. Chen, and K.-F. Huang on this manuscript. The financial support came from the National Science and Technology Council under Grants 108-2611-M-001-006-MY3 and 111-2611-M-001-006-MY3 as well as the Investigator Award AS-IA-110-M03 from Academia Sinica to T.-Y. Ho.

References

Andreae, M. O. (1983). Soot carbon and excess fine potassium: Long-range transport of combustion-derived aerosols. *Science*, *220*(4602), 1148–1151. https://doi.org/10.1126/science.220.4602.1148

Baker, A. R., & Jickells, T. D. (2006). Mineral particle size as a control on aerosol iron solubility. *Geophysical Research Letters*, *33*(17). https://doi.org/10.1029/2006gl026557

Basha, S. I., Aziz, A., Maslehuddin, M., Ahmad, S., Hakeem, A. S., & Rahman, M. M. (2020). Characterization, processing, and application of heavy fuel Oil Ash, an industrial waste material—a review. *The Chemical Record*, *20*(12), 1568–1595. https://doi.org/10.1002/tcr.202000100

Beard, B. L., Johnson, C. M., Von Damm, K. L., & Poulson, R. L. (2003). Iron isotope constraints on Fe cycling and mass balance in oxygenated Earth oceans. *Geology*, *31*(7), 629. https://doi.org/10.1130/0091-7613(2003)031<0629:Iicofc>2.0.Co;2

Buck, C. S., Aguilar-Islas, A., Marsay, C., Kadko, D., & Landing, W. M. (2019). Trace element concentrations, elemental ratios, and enrichment factors observed in aerosol samples collected during the US GEOTRACES eastern Pacific Ocean transect (GP16). *Chemical Geology*, *511*, 212–224. https://doi.org/10.1016/j.chemgeo.2019.01.002

Buck, C. S., Landing, W. M., Resing, J. A., & Lebon, G. T. (2006). Aerosol iron and aluminum solubility in the northwest Pacific Ocean: Results from the 2002 IOC cruise. *Geochemistry, Geophysics, Geosystems*, *7*(4). https://doi.org/10.1029/2005gc000977

Conway, T. M., Hamilton, D. S., Shelley, R. U., Aguilar-Islas, A. M., Landing, W. M., Mahowald, N. M., & John, S. G. (2019). Tracing and constraining anthropogenic aerosol iron fluxes to the North Atlantic Ocean using iron isotopes. *Nature Communications*, *10*(1), 2628. https://doi.org/10.1038/s41467-019-10457-w

Craddock, P. R., & Dauphas, N. (2010). Iron isotopic compositions of geological reference materials and chondrites. *Geostandards and Geoanalytical Research*, *35*(1), 101–123. https://doi.org/10.1111/j.1751-908X.2010.00085.x

Cutter, G., Casciotti, K., Croot, P. L., Geibert, W., Heimburger, L.-E., Lohan, M. C., & van de Flierdt, T. (2017). Sampling and sample-handling protocols for GEOTRACES cruises. *3*. https://doi.org/10.25607/OBP-2

Dauphas, N., John, S. G., & Rouxel, O. (2017). Iron isotope systematics. *Reviews in Mineralogy and Geochemistry*, *82*(1), 415–510. https://doi.org/10.2138/rmg.2017.82.11

Duce, R. A., Liss, P. S., Merrill, J. T., Atlas, E. L., Buat-Menard, P., Hicks, B. B., et al. (1991). The atmospheric input of trace species to the world ocean. *Global Biogeochemical Cycles*, *5*(3), 193–259. https://doi.org/10.1029/91gb01778

Eggimann, D. W., & Betzer, P. R. (1976). Decomposition and analysis of refractory oceanic suspended materials. *Analytical Chemistry*, *48*(6), 886–890. https://doi.org/10.1021/ac60370a005

Fitzsimmons, J. N., & Conway, T. M. (2023). Novel insights into marine Iron biogeochemistry from iron isotopes. *Annual Review of Marine Science*, *15*(1), 383–406. https://doi.org/10.1146/annurev-marine-032822-103431

Gong, Y., Xia, Y., Huang, F., & Yu, H. (2016). Average iron isotopic compositions of the upper continental crust: Constrained by loess from the Chinese loess plateau. *Acta Geochimica*, *36*(2), 125–131. https://doi.org/10.1007/s11631-016-0131-5

Ho, T.-Y., & Hsieh, C.-C. (2024). The iron isotopic composition and the elemental ratios (Cd/Ti) in the size-fractionated aerosols collected over the East China Sea [Dataset]. *Dryad*. https://doi.org/10.5061/dryad.rv15dv4h3

Hsieh, C.-C., Chen, H.-Y., & Ho, T.-Y. (2022). The effect of aerosol size on Fe solubility and deposition flux: A case study in the East China sea. *Marine Chemistry*, *241*, 104106. https://doi.org/10.1016/j.marchem.2022.104106

Hsieh, C.-C., You, C.-F., & Ho, T.-Y. (2023). The solubility and deposition flux of East Asian aerosol metals in the East China Sea: The effects of Aeolian transport processes. *Marine Chemistry*, *253*, 104268. https://doi.org/10.1016/j.marchem.2023.104268

Hu, Z. C., & Gao, S. (2008). Upper crustal abundances of trace elements: A revision and update. *Chemical Geology*, *253*(3–4), 205–221. https://doi.org/10.1016/j.chemgeo.2008.05.010

Jickells, T. D., Baker, A. R., & Chance, R. (2016). Atmospheric transport of trace elements and nutrients to the oceans. *Philosophical Transactions A: Mathematical, Physical and Engineering Sciences*, *374*(2081), 20150286. https://doi.org/10.1098/rsta.2015.0286

Kurisu, M., Adachi, K., Sakata, K., & Takahashi, Y. (2019). Stable isotope ratios of combustion Iron produced by evaporation in a steel plant. *ACS Earth and Space Chemistry*, *3*(4), 588–598. https://doi.org/10.1021/acsearthspacechem.8b00171

Kurisu, M., Sakata, K., Miyamoto, C., Takaku, Y., Iizuka, T., & Takahashi, Y. (2016). Variation of Iron isotope ratios in anthropogenic materials emitted through combustion processes. *Chemistry Letters*, *45*(8), 970–972. https://doi.org/10.1246/cl.160451

Kurisu, M., Sakata, K., Uematsu, M., Ito, A., & Takahashi, Y. (2021). Contribution of combustion Fe in marine aerosols over the Northwestern Pacific estimated by Fe stable isotope ratios. *Atmospheric Chemistry and Physics Discussions*, *2021*, 1–32. https://doi.org/10.5194/acp-2021-460

Kurisu, M., & Takahashi, Y. (2019). Testing Iron stable isotope ratios as a signature of biomass burning. *Atmosphere*, *10*(2), 76. https://doi.org/10.3390/atmos10020076

Kurisu, M., Takahashi, Y., Iizuka, T., & Uematsu, M. (2016). Very low isotope ratio of iron in fine aerosols related to its contribution to the surface ocean. *Journal of Geophysical Research: Atmospheres*, *121*(18), 11119–11136. https://doi.org/10.1002/2016jd024957

Lam, P. J., & Bishop, J. K. B. (2008). The continental margin is a key source of iron to the HNLC North Pacific Ocean. *Geophysical Research Letters*, *35*(7). https://doi.org/10.1029/2008gl033294

Lin, Y.-C., Chen, J.-P., Ho, T.-Y., & Tsai, I.-C. (2015). Atmospheric iron deposition in the northwestern Pacific Ocean and its adjacent marginal seas: The importance of coal burning. *Global Biogeochemical Cycles*, *29*(2), 138–159. https://doi.org/10.1002/2013gb004795

Lin, Y. C., Yu, M., Xie, F., & Zhang, Y. (2022). Anthropogenic emission sources of sulfate aerosols in Hangzhou, East China: Insights from isotope techniques with consideration of fractionation effects between gas-to-particle transformations. *Environmental Science & Technology*, *56*(7), 3905–3914. https://doi.org/10.1021/acs.est.1c05823

Luo, C., Mahowald, N., Bond, T., Chuang, P. Y., Artaxo, P., Siefert, R., & Schauer, J. (2008). Combustion iron distribution and deposition. *Global Biogeochemical Cycles*, *22*(1). https://doi.org/10.1029/2007gb002964

Marsay, C. M., Kadko, D., Landing, W. M., & Buck, C. S. (2022). Bulk aerosol trace element concentrations and deposition fluxes during the U.S. GEOTRACES GP15 pacific meridional transect. *Global Biogeochemical Cycles*, *36*(2). https://doi.org/10.1029/2021gb007122

Martin, J. H. (1990). Glacial-interglacial CO_2 change: The iron hypothesis. *Paleoceanography*, *5*(1), 1–13. https://doi.org/10.1029/PA005i001p00001

Mead, C., Herckes, P., Majestic, B. J., & Anbar, A. D. (2013). Source apportionment of aerosol iron in the marine environment using iron isotope analysis. *Geophysical Research Letters*, *40*(21), 5722–5727. https://doi.org/10.1002/2013gl057713

Meskhidze, N., Völker, C., Al-Abadleh, H. A., Barbeau, K., Bressac, M., Buck, C., et al. (2019). Perspective on identifying and characterizing the processes controlling iron speciation and residence time at the atmosphere-ocean interface. *Marine Chemistry*, *217*, 103704. https://doi.org/10.1016/j.marchem.2019.103704

Morton, P. L., Landing, W. M., Hsu, S.-C., Milne, A., Aguilar-Islas, A. M., Baker, A. R., et al. (2013). Methods for the sampling and analysis of marine aerosols: Results from the 2008 GEOTRACES aerosol intercalibration experiment. *Limnology and Oceanography: Methods*, *11*(2), 62–78. https://doi.org/10.4319/lom.2013.11.62

Myriokefalitakis, S., Ito, A., Kanakidou, M., Nenes, A., Krol, M. C., Mahowald, N. M., et al. (2018). Reviews and syntheses: The GESAMP atmospheric iron deposition model intercomparison study. *Biogeosciences*, *15*(21), 6659–6684. https://doi.org/10.5194/bg-15-6659-2018

Nishioka, J., Ono, T., Saito, H., Nakatsuka, T., Takeda, S., Yoshimura, T., et al. (2007). Iron supply to the Western subarctic Pacific: Importance of iron export from the Sea of Okhotsk. *Journal of Geophysical Research*, *112*(C10). https://doi.org/10.1029/2006jc004055

Nriagu, J. O., & Pacyna, J. M. (1988). Quantitative assessment of worldwide contamination of air, water and soils by trace metals. *Nature*, *333*(6169), 134–139. https://doi.org/10.1038/333134a0

Perron, M. M. G., Meyerink, S., Corkill, M., Strzelec, M., Proemse, B. C., Gault-Ringold, M., et al. (2022). Trace elements and nutrients in wildfire plumes to the southeast of Australia. *Atmospheric Research*, *270*, 106084. https://doi.org/10.1016/j.atmosres.2022.106084

Perron, M. M. G., Strzelec, M., Gault-Ringold, M., Proemse, B. C., Boyd, P. W., & Bowie, A. R. (2020). Assessment of leaching protocols to determine the solubility of trace metals in aerosols. *Talanta*, *208*, 120377. https://doi.org/10.1016/j.talanta.2019.120377

Pinedo-Gonzalez, P., Hawco, N. J., Bundy, R. M., Armbrust, E. V., Follows, M. J., Cael, B. B., et al. (2020). Anthropogenic Asian aerosols provide Fe to the North Pacific Ocean. *Proceedings of the National Academy of Sciences of the U S A*, *117*(45), 27862–27868. https://doi.org/10.1073/pnas.2010315117

Resing, J. A., Sedwick, P. N., German, C. R., Jenkins, W. J., Moffett, J. W., Sohst, B. M., & Tagliabue, A. (2015). Basin-scale transport of hydrothermal dissolved metals across the South Pacific Ocean. *Nature*, *523*(7559), 200–203. https://doi.org/10.1038/nature14577

Rouxel, O. J., & Auro, M. (2010). Iron isotope variations in coastal seawater determined by multicollector ICP-MS. *Geostandards and Geoanalytical Research*, *34*(2), 135–144. https://doi.org/10.1111/j.1751-908X.2010.00063.x

Sarthou, G., Baker, A. R., Blain, S., Achterberg, E. P., Boye, M., Bowie, A. R., et al. (2003). Atmospheric iron deposition and sea-surface dissolved iron concentrations in the eastern Atlantic Ocean. *Deep Sea Research Part I: Oceanographic Research Papers*, *50*(10–11), 1339–1352. https://doi.org/10.1016/s0967-0637(03)00126-2

Sedwick, P. N., Sholkovitz, E. R., & Church, T. M. (2007). Impact of anthropogenic combustion emissions on the fractional solubility of aerosol iron: Evidence from the Sargasso Sea. *Geochemistry, Geophysics, Geosystems*, *8*(10). https://doi.org/10.1029/2007gc001586

Sholkovitz, E. R., Sedwick, P. N., & Church, T. M. (2009). Influence of anthropogenic combustion emissions on the deposition of soluble aerosol iron to the ocean: Empirical estimates for island sites in the North Atlantic. *Geochimica et Cosmochimica Acta*, *73*(14), 3981–4003. https://doi.org/10.1016/j.gca.2009.04.029

Sieber, M., Conway, T. M., de Souza, G. F., Hassler, C. S., Ellwood, M. J., & Vance, D. (2021). Isotopic fingerprinting of biogeochemical processes and iron sources in the iron-limited surface Southern Ocean. *Earth and Planetary Science Letters*, *567*, 116967. https://doi.org/10.1016/j.epsl.2021.116967

Stevenson, E. I., Fantle, M. S., Das, S. B., Williams, H. M., & Aciego, S. M. (2017). The iron isotopic composition of subglacial streams draining the Greenland ice sheet. *Geochimica et Cosmochimica Acta*, *213*, 237–254. https://doi.org/10.1016/j.gca.2017.06.002

Streibel, T., Schnelle-Kreis, J., Czech, H., Harndorf, H., Jakobi, G., Jokiniemi, J., et al. (2017). Aerosol emissions of a ship diesel engine operated with diesel fuel or heavy fuel oil. *Environmental Science and Pollution Research International*, *24*(12), 10976–10991. https://doi.org/10.1007/s11356-016-6724-z

Tagliabue, A., Bowie, A. R., Boyd, P. W., Buck, K. N., Johnson, K. S., & Saito, M. A. (2017). The integral role of iron in ocean biogeochemistry. *Nature*, *543*(7643), 51–59. https://doi.org/10.1038/nature21058

Waeles, M., Baker, A. R., Jickells, T., & Hoogewerff, J. (2007). Global dust teleconnections: Aerosol iron solubility and stable isotope composition. *Environmental Chemistry*, *4*(4), 233. https://doi.org/10.1071/en07013

Wang, B.-S., & Ho, T.-Y. (2020). Aerosol Fe cycling in the surface water of the Northwestern Pacific ocean. *Progress in Oceanography*, *183*, 102291. https://doi.org/10.1016/j.pocean.2020.102291